and amplitude m, habit plane normal **h**, and orientation relationship between parent and product phases (Table 3). The habit plane of the reference variant is $(557)_\gamma$. Concerning the orientation relationship, the close-packed planes are not exactly parallel, as quoted in literature, e.g., [47].

The habit plane and shape strain direction were calculated for the 24 possible variants which may form in a given austenite grain. The corresponding habit plane and $\{001\}_\alpha$ poles are plotted in Fig. 10 in the $\langle 001\rangle_\gamma$ frame of the parent austenite phase. The orientation relationships between variants were also calculated together with their number fractions, under a "no local variant selection" assumption. The results are reported in Table 4. The corresponding misorientation angle histogram is reported with the "Kelly" label in Fig. 6(b), which does not greatly differ from those obtained with KS and NW. In fact, the Kelly orientation relationship is between the KS and NW orientation relationships. In the following, only the habit plane indices and shape strain are used, but the orientation relationships between austenite and bainite were experimentally observed to cluster within a few degrees around the "Kelly" one.

Table 4
Misorientation relationships between two bainite variants within the same austenite grain as given by the γ/α orientation relationship listed in Table 3

Misorientation angle (°)	Low-index axis family	Offset (°)	Pairs of variants
0.0	–	–	1–1
4.7	$\{011\}_\alpha$	4.0	1–2
11.9	$\{133\}_\alpha$	1.6	1–10
14.1	$\{023\}_\alpha$	3.6	1–3, 1–5
16.6	$\{133\}_\alpha$	0.9	1–7
19.9	$\{014\}_\alpha$	5.5	1–22
19.9	$\{014\}_\alpha$	3.6	1–4
49.3	$\{111\}_\alpha$	4.1	1–20
50.0	$\{334\}_\alpha$	3.8	1–18, 1–19
50.5	$\{133\}_\alpha$	1.6	1–16, 1–17
50.8	$\{233\}_\alpha$	0.1	1–21
52.3	$\{133\}_\alpha$	3.5	1–6, 1–8
55.0	$\{133\}_\alpha$	1.9	1–9, 1–11
55.4	$\{011\}_\alpha$	0.3	1–24
56.8	$\{133\}_\alpha$	2.9	1–14, 1–15
60.0	$\{011\}_\alpha$	0.3	1–12, 1–13
60.3	$\{334\}_\alpha$	2.2	1–23

"Offset" is the angle between the actual rotation axis and the closest low-index axis.

4.2.2. Modelling self-accommodation between two bainite variants

To qualitatively represent the highly intricate configuration of variants, a micromechanical, self-consistent scheme was used together with the Eshelby inclusion method [48]. This model enables to calculate mean stress and strain fields within each of the three phases. However, it does not take into account interface phenomena. Four pairs of variants were chosen to represent the spatial and crystallographic features observed in upper bainite and martensite microstructures. They are listed in Table 5. Calculations were carried out using a house-made computer program for reference variant 1 formed together with any of variants 1, 2, 10, or 23. Variants 1 and 2 have close habit planes and a low misorientation angle. Variants 1 and 10 have almost perpendicular habit planes and a low misorientation angle. Variants 1 and 23 have the same habit plane but are highly misoriented (5.6° from the twin misorientation relationship).

Use of the Eshelby inclusion method enables to take into account the geometry of the phases. The austenite phase was assumed to be isotropic. Each of the "plate-like" bainite variants (in fact, each set of parallel groups as explained before) was modelled as a flat ellipsoidal inclusion having a shape ratio of 1:20, consistently with experimental observations, and minor axis normal to its habit plane. The ellipsoid shape allows the stresses and strains to be homogeneous in the inclusion. The volume fractions of phases were 0.25 for the first variant, 0.25 for the second variant, and 0.5 for untransformed austenite, consistently with metallographic observation of many partially transformed bainite packets (e.g., Fig. 3(a)).

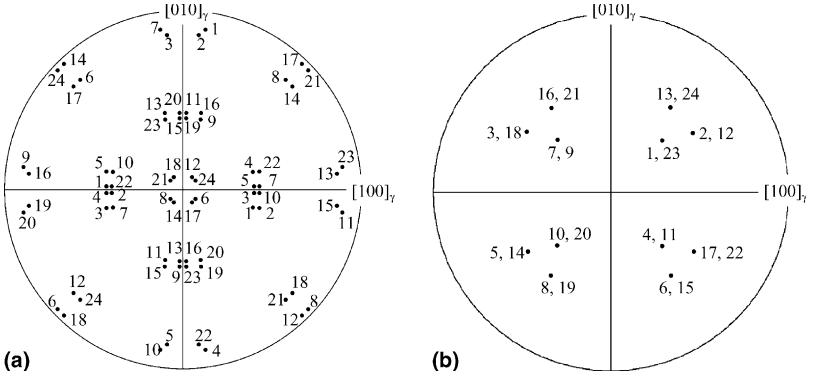

Fig. 10. (a) $\{001\}_\alpha$ and (b) $\{557\}_\gamma$ habit plane pole figures calculated using the PTMC model. Numbers refer to the 24 possible variants.